Inorganic Chemistry
Cite This: Inorg. Chem. 2019, 58, 15320−15329
Article
pubs.acs.org/IC

Picosecond to Nanosecond Manipulation of Excited-State Lifetimes in Complexes with an Fe^{II} to Ti^{IV} Metal-to-Metal Charge Transfer: The Role of Ferrocene Centered Excited States

Maksim Y. Livshits,[†] Michael D. Turlington,[‡] Carl O. Trindle,[§] Lei Wang,[†] Zikri Altun,[∥] Paul S. Wagenknecht,*[,‡] and Jeffrey J. Rack*[,†]

[†]Department of Chemistry and Chemical Biology, University of New Mexico, Albuquerque, New Mexico 87131, United States
[‡]Department of Chemistry, Furman University, Greenville, South Carolina 29613, United States
[§]Department of Chemistry, University of Virginia, Charlottesville, Virginia 22904, United States
[∥]Department of Physics, Marmara University, Göztepe Kampus, 34772 Istanbul, Turkey

Supporting Information

ABSTRACT: Time-resolved transient absorption spectroscopy and computational analysis of D−π−A complexes comprising Fe^{II} donors and Ti^{IV} acceptors with the general formula $^{R}Cp_2Ti(C_2Fc)_2$ (where ^{R}Cp = Cp*, Cp, and $^{MeOOC}Cp$) and $^{TMS}Cp_2Ti(C_2Fc)(C_2R)$ (where R = Ph or CF_3) are reported. The transient absorption spectra are consistent with an Fe^{III}/Ti^{III} metal-to-metal charge-transfer (MMCT) excited state for all complexes. Thus, excited-state decay is assigned to back-electron transfer (BET), the lifetime of which ranges from 18.8 to 41 ps. Though spectroscopic analysis suggests BET should fall into the Marcus inverted regime, the observed kinetics are not consistent with this assertion. TDDFT calculations reveal that the singlet metal-to-metal charge-transfer (^{1}MMCT) excited state for the Fe^{II}/Ti^{IV} complexes is not purely MMCT in nature but is contaminated with the higher-energy ^{1}Fc (d-d) state. For the diferrocenyl complexes, $^{R}Cp_2Ti(C_2Fc)_2$, the ratio of MMCT to Fc centered character ranges from 57:43 for the Cp* complex to 85:15 for the $^{MeOOC}Cp$ complex. For the diferrocenyl and monoferrocenyl complexes investigated herein, the excited-state lifetimes decrease with increased ^{1}Fc character. The effect of Cu^I coordination was also analyzed by time-resolved transient absorption spectroscopy and reveals the elongation of the excited-state lifetime by 3 orders of magnitude to 63 ns. The transient spectra and TDDFT analysis suggest that the long-lived excited state in $Cp_2Ti(C_2Fc)_2$·CuX (where X is Cl or Br) is a triplet iron species with an electron arrangement of Ti^{IV}−$^3Fe^{II}$−Cu^I.

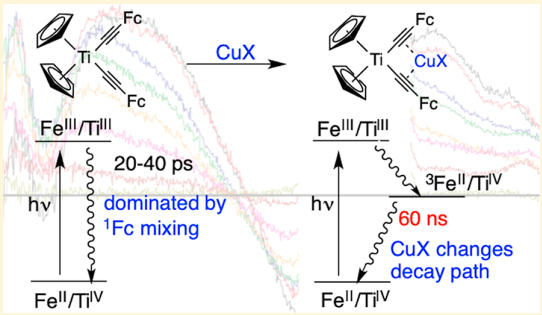

INTRODUCTION

Charge-transfer excited states where electron hole pairs are separated over large distances have received much attention for their applications in solar energy conversion,[1−3] photoredox catalysis,[4,5] molecular spintronics,[6] and nonlinear optical materials.[7] Typically, expensive second- and third-row transition metals (e.g., Ru^{II},[1,2,4,8,9] Re^{I},[9−11] Rh^{II},[12] Ir^{III},[4,13] and Pt^{II}[4,9−11]) have been employed in metal-to-ligand charge-transfer (MLCT) studies due to their long excited-state lifetimes as well as photostability. Cheaper earth-abundant first-row transition metals (e.g., Cr^{III},[14] Fe^{II},[15−17] $Co^{III/II}$,[18,19] and Cu^{I}[21]) have also been investigated for the same applications. Unfortunately, first-row transition metals typically do not perform as well as their second- and third-row counterparts due to the presence of low-lying, thermally accessible metal centered states, which can rapidly deactivate the charge-transfer excited state and contribute to poor photostability.[14,22−26] However, more recently, first-row transition metal complexes have been developed with performance characteristics approaching that of parallel second- and third-row transition metal sensitizers.[14,16,17,19−21,27−38]

Our recent investigations of possible first-row transition metal sensitizers have focused on a series of D−π−A complexes with Fe^{II} donors and Ti^{IV} acceptors (Figure 1).[39,40] A Marcus−Hush type analysis of the electrochemical and spectroscopic data is consistent with the assignment of the low-energy absorption (540−630 nm) as an $Fe^{II} \rightarrow Ti^{IV}$ metal-to-metal charge-transfer (MMCT) band.[40] Chiefly, good agreement was observed between $\Delta E_{1/2}$ ($E_{1/2}$ ($Fc^{+/0}$) − $E_{1/2}$ ($Ti^{IV/III}$)) and the spectroscopically determined value for $\Delta G°$. TDDFT calculations supported this hypothesis, but also indicated some Fe centered d-d character mixed into this MMCT band. Of particular significance is that the excited-state ($ES^{+/0}$) potential for this series of Fe^{II}/Ti^{IV} complexes is estimated to be more negative than ∼−1.3 V vs $FcH^{+/0}$,

Received: July 31, 2019
Published: November 5, 2019

DOI: 10.1021/acs.inorgchem.9b02316
Inorg. Chem. 2019, 58, 15320−15329

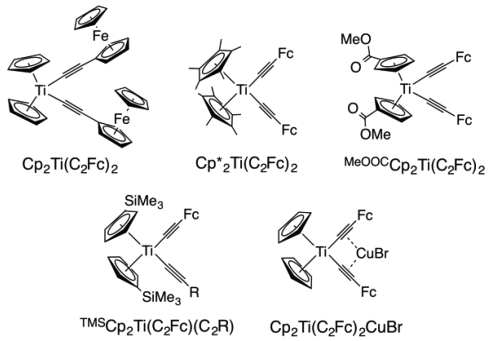

Figure 1. Fe^{II}–Ti^{IV} complexes discussed in this paper along with abbreviations used. $^{R}Cp_2Ti(C_2Fc)_2$ is the abbreviation used to refer to the complexes with two ethynylferrocene ligands and any substitution on the Cp ring (top row).

suggesting that such D–π–A complexes might be potent excited-state reducing agents. One obstacle to using these systems as excited-state reductants is the instability of the $1e^-$ oxidized forms. However, binding Cu^I between the alkynes (e.g., $Cp_2Ti(C_2Fc)_2CuBr$, Figure 1) stabilizes these complexes to oxidation while maintaining the MMCT transition.[39] Herein, we continue investigation of the Fe^{II}/Ti^{IV} D–π–A complexes by examining the excited-state dynamics. Previous spectroscopic data demonstrated that the ground-state Fe^{II}/Ti^{IV} and excited-state Fe^{III}/Ti^{III} potential wells are nested; thus back-electron transfer (BET) rates from the MMCT state are expected to be consistent with the Marcus inverted region (Figure 2). To test this hypothesis, we have expanded the set

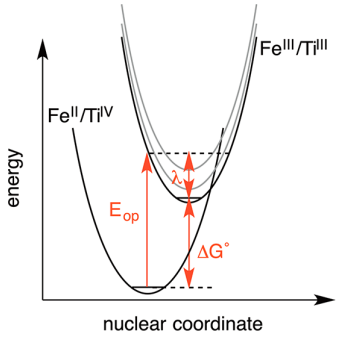

Figure 2. Potential-well diagram showing the Fe^{II}/Ti^{IV} ground state and Fe^{III}/Ti^{III} excited state (black curves), and the relationship between the spectroscopic parameters, E_{op}, λ, and the free energy for BET, $-\Delta G°$. Gray curves represent Fe^{III}/Ti^{III} excited states at increasing energy, showing that the activation energy for BET increases for higher-energy MMCT states, predicting longer excited-state lifetimes for higher-energy MMCT states.

of $^{R}Cp_2Ti(C_2Fc)_2$ complexes by preparing $^{MeOOC}Cp_2Ti(C_2Fc)_2$. The electron-poor nature of the esterified Cp ring anodically shifts the $Ti^{IV/III}$ potential, thus lowering the magnitude of $\Delta G°$, providing a larger thermodynamic range over which to investigate the rate of BET as a function of $\Delta G°$. However, BET kinetics consistent with the Marcus inverted region were not observed. Instead, excited-state lifetimes appear to be dominated by mixing with the ^{1}Fc d-d excited state. We conclude this study by commenting on the effect that the coordination of Cu^I plays on the excited-state dynamics, chiefly, that it *extends the excited-state lifetime by 3 orders of magnitude*. In this case, the ^{3}Fc state appears to dominate the decay kinetics.

RESULTS AND DISCUSSION

Steady-State Absorption Spectroscopy and Marcus–Hush Analysis. As expected for an $Fe^{II} \rightarrow Ti^{IV}$ MMCT, the energy of this transition decreases as the $Ti^{IV/III}$ reduction potential shifts anodically.[40] Modulation of the $Ti^{IV/III}$ reduction potential and the resulting MMCT transition energy is accomplished by modification of the substituents on the Cp ring for the $^{R}Cp_2Ti(C_2Fc)_2$ complexes (Figure 3). As

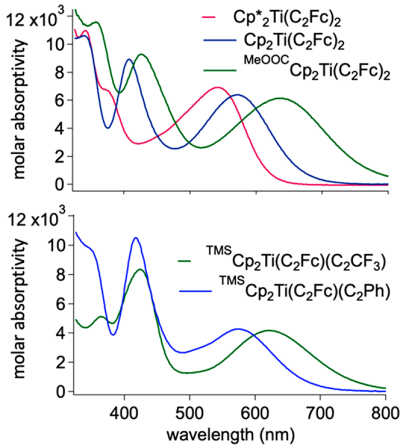

Figure 3. UV–vis absorption spectra in THF for bis-ferrocenyl complexes (top) and monoferrocenyl complexes (bottom). The color of the curves approximates the color of each complex.

previously reported,[40] the MMCT band for the more electron-rich Cp* complex ($E_{1/2}$ ($Ti^{IV/III}$) = −2.28 V vs $Fc^{+/0}$) is significantly blue-shifted relative to that of the Cp complex ($E_{1/2}$ ($Ti^{IV/III}$) = −1.75 V vs $Fc^{+/0}$).

Herein, we report the synthesis and characterization of $^{MeOOC}Cp_2Ti(C_2Fc)_2$. As expected, the e^- withdrawing groups diminish the e^- density on Ti ($E_{1/2}$ ($Ti^{IV/III}$) = −1.46 V vs $Fc^{+/0}$) (Supporting Information, Figure S1), which results in a concomitant red-shift of the MMCT band (Figure 3). The energy of the optical transition, E_{op}, for the $^{MeOOC}Cp$, Cp, and Cp* complexes in THF is 15720, 17510, and 18450 cm^{-1}, respectively. Likewise, for the previously reported monoferrocenyl complexes,[40] $^{TMS}Cp_2Ti(C_2Fc)(C_2R)$, the MMCT band of the complex with R = CF_3 is red-shifted with respect to the complex with R = Ph (16050 vs 17450 cm^{-1}, respectively). Lastly, the band between 370 and 440 nm (Figure 3) is assigned to a Cp → Ti^{IV} LMCT.[40,41]

The spectroscopic data and Marcus–Hush analysis (Supporting Information, Table S1) for the complexes shown in Figure 1 clearly demonstrate that the reorganization energy (λ, determined from $\Delta\nu_{1/2}$ of the MMCT band) is significantly less than $-\Delta G°$ for BET from the excited state (Figure 2). Namely, $-\Delta G°$ is between 10900 and 15900 cm^{-1} and λ is between 2600 and 5200 cm^{-1}. As previously mentioned, this suggests that BET from the Fe^{III}/Ti^{III} excited state should fall in the Marcus inverted region. Thus, for the bis-ferrocenyl complexes, the observed excited-state lifetimes are expected to increase in the order $^{MeOOC}Cp_2Ti(C_2Fc)_2$ < $Cp_2Ti(C_2Fc)_2$ < $Cp^*_2Ti(C_2Fc)_2$. Similarly, for the monoferrocenyl complexes, $^{TMS}Cp_2Ti(C_2Fc)(C_2Ph)$ is expected to

DOI: 10.1021/acs.inorgchem.9b02316
Inorg. Chem. 2019, 58, 15320–15329

have a shorter excited-state lifetime than $^{TMS}Cp_2Ti(C_2Fc)(C_2CF_3)$.

Experimental Excited-State Dynamics. Ultrafast pump−probe transient absorption spectroscopy was utilized to characterize the Fe^{III}/Ti^{III} MMCT excited-state lifetimes (Figure 4C). The steady-state electronic absorption spectrum of $Cp_2Ti(C_2Fc)_2$ (Figure 4A, same as Figure 3) as well as the reduced $Cp_2Ti(C_2Fc)_2$ and oxidized HC_2Fc (from spectroelectrochemistry, Figure 4B) aid in assigning the transient features. As mentioned above, the $1e^-$ oxidized $Cp_2Ti(C_2Fc)_2$ complex is not stable, and thus, the absorption spectrum of oxidized HC_2Fc is used to help assign excited-state absorption features. The transient spectra and global analysis for the other complexes shown in Figure 1 are found in the Supporting Information (Figures S5−S14).

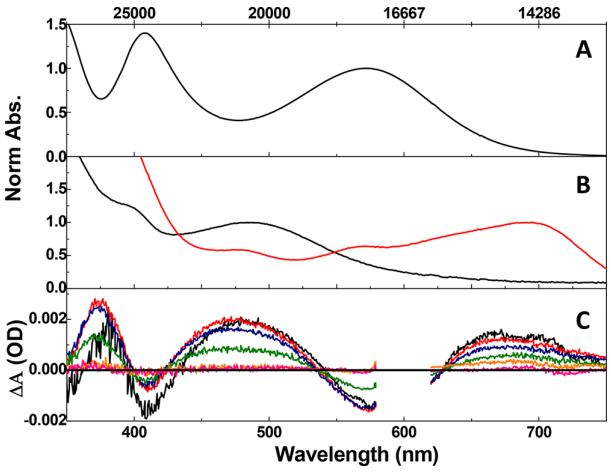

Figure 4. (A) Electronic absorbance spectrum of $Cp_2Ti(C_2Fc)_2$. (B) Electronic absorbance of reduced $Cp_2Ti(C_2Fc)_2$ (black) and oxidized HC_2Fc (red). (C) Select transient spectra of $Cp_2Ti(C_2Fc)_2$ with 600 nm excitation at time delays of 0.32 (black), 1.5 (red), 6.0 (blue), 24 (green), 96 (orange), and 180 ps (pink). The laser line for the pump−probe data has been removed, and a reference zero line has been added for ease of interpretation.

One e^- reduction of $Cp_2Ti(C_2Fc)_2$ (Figure 4B) reveals a new broad transition at 485 nm which we assign to a $Ti^{III} \rightarrow$ Cp or $Ti^{III} \rightarrow C_2Cp$ MLCT. Absorbance between 450 and 500 nm for Cp_2Ti^{III} complexes is precedented, having been assigned to CT for $[Cp_2TiX]_2$ dimers.[42] One e^- oxidation of HC_2Fc reveals a feature at 680 nm (Figure 4B) that we assign to a $C_2Cp \rightarrow Fe^{III}$ LMCT based on similar assignments for ethynylferrocene substituents.[43] All higher-energy transitions (λ < 450 nm) in both oxidized HC_2Fc and reduced $Cp_2Ti(C_2Fc)_2$ are likely due to $\pi \rightarrow \pi^*$ transitions in C_2Cp or Cp. Finally, the pump−probe transient spectra (Figure 4C) feature three induced absorptions as well as the loss of two absorptions (bleaches). The correspondence of the bleaches (negative absorptions) with the steady-state absorbance suggests the bleach at ∼580 nm can be assigned to loss of the $Fe^{II} \rightarrow Ti^{IV}$ MMCT and the bleach at 412 nm to loss of the Cp $\rightarrow Ti^{IV}$ LMCT. The spectroelectrochemistry suggests assignment of the induced excited-state absorption from 430 to 540 nm to $Ti^{III} \rightarrow$ Cp or $Ti^{III} \rightarrow C_2Cp$ MLCT and that the excited-state absorption from 630 to >750 nm contains contributions from $C_2Cp \rightarrow Fe^{III}$ LMCT. Thus, the observed transient spectra are consistent with a Ti^{III}/Fe^{III} MMCT excited state. The highest-energy excited-state absorption (<400 nm) is likely caused by higher-lying MLCT transitions and/or Cp or C_2Cp $\pi \rightarrow \pi^*$ transitions. The complexes $Cp^*_2Ti(C_2Fc)_2$, $Cp_2Ti(C_2Fc)_2$, $^{MeOOC}Cp_2Ti(C_2Fc)_2$, $^{TMS}Cp_2Ti(C_2Fc)(C_2Ph)$, and $^{TMS}Cp_2(C_2Fc)(C_2CF_3)$ show similar spectral features (Figures S5−S14).

The single-wavelength kinetic traces and singular value decomposition (SVD) global-fitting analysis for $Cp^*_2Ti(C_2Fc)_2$, $Cp_2Ti(C_2Fc)_2$, $^{MeOOC}Cp_2Ti(C_2Fc)_2$, $^{TMS}Cp_2Ti(C_2Fc)(C_2Ph)$, and $^{TMS}Cp_2(C_2Fc)(C_2CF_3)$ reveal a monoexponential decay (Figures S5−S14) ascribed to BET from the Fe^{III}/Ti^{III} excited state to the Fe^{II}/Ti^{IV} ground state. The lifetimes for BET range from 18.8 to 41 ps (Table 1). An occasional subpicosecond time constant (∼0.5 ps) is also observed in single-wavelength kinetic fitting yet is not necessary in global kinetic fits. This 0.5 ps time constant is ascribed to solvent reorganization based on the precedence of previously reported D−π−A complexes with Fc donors.[44] The observation that both the lifetimes for BET and the trend of lifetime vs $\Delta G°$ (though with a limited data set) are similar for the monoferrocenyl and diferrocenyl complexes suggests that excited-state Fe^{II}/Fe^{III} intervalence charge-transfer (IVCT) interactions in the $Fe^{III}−Ti^{III}−Fe^{II}$ excited state do not significantly affect the decay kinetics of the diferrocenyl complexes. Furthermore, our previous investigations showed no evidence of ground-state $Fe^{III}−Ti^{IV}−Fe^{II}$ IVCT in the one e^- oxidized $Cp_2Ti(C_2Fc)_2CuBr$ complex.[39]

Similar excited-state absorptions and decay constants were reported for 4-(ferrocen-1-yl)benzylidene-malononitrile (Fc-ph-DCV), another D−π−A complex with a Fc donor.[44] Fluorescence upconversion and pump−probe transient absorption spectroscopy of Fc-ph-DCV in CH_3CN yielded lifetimes (τ_1 to τ_3) of 110 ± 30 fs, 600 ± 100 fs, and 49 ± 3 ps, as well as two broad photoinduced excited-state absorptions (from <450 to 530 nm and from 600 to >750 nm). A ground-state bleach (530−600 nm) was observed at the same wavelength as the Fe^{II}-to-acceptor (d $\rightarrow \pi^*$) CT band.

Table 1. Transient Lifetimes, Thermodynamics for BET from the MMCT State, and Computational Data for the MMCT State

compound	lifetime (ps)[a]	$\Delta G°$ (eV)	λ_{max} (nm) (exp (calc))	NTO pairs (dom:min[b])	CT indices	
					Q_{CT}	D_{CT}[c]
$Cp^*_2Ti(C_2Fc)_2$	18.8 (0.8)	−1.97	542 (544)	57:43	0.60	0.96
$Cp_2Ti(C_2Fc)_2$	26 (1)	−1.66	571 (562)	70:30	0.64	1.35
$^{MeOOC}Cp_2Ti(C_2Fc)_2$	41 (1)	−1.35	636 (596)	85:15	0.70	2.11
$^{TMS}Cp_2Ti(C_2Fc)(C_2Ph)$	24 (1)	−1.59	573 (564)	87:13	0.67	3.50
$^{TMS}Cp_2Ti(C_2Fc)(C_2CF_3)$	32 (4)	−1.36	623 (586)	93:7	0.72	4.15

[a]Values in parentheses are the standard error. [b]dom = the percentage contribution from the dominant hole-particle pair; min = the sum of the contributions from the remaining hole-particle pairs. [c]In Å.

DOI: 10.1021/acs.inorgchem.9b02316
Inorg. Chem. 2019, 58, 15320−15329

Observed time constants were assigned to $S_2 \rightarrow S_1$ internal conversion (τ_1) (as they were limited to excitation at 390 nm), solvent reorganization (τ_2), and BET from S_1 to S_0 (τ_3). The observed excited-state absorptions were correlated to S_1. The coincidence of a 600 to >750 nm excited-state absorption in both the Fc-ph-DCV and the Fe^{II}/Ti^{IV} complexes reported herein provides additional evidence that oxidized Fc contributes to this signal and therefore supports the assignment of the measured lifetimes to BET from the Fe^{III}/Ti^{III} excited state.

As mentioned in the Introduction, spectroscopic analysis of the ground-state MMCT transition suggests that BET from the Ti^{III}/Fe^{III} excited state should fall into the Marcus inverted region. However, the observed lifetimes (Table 1) are not consistent with that prediction. Chiefly, for the diferrocenyl complexes (top three entries in Table 1) there is a decrease in the lifetime for BET as the driving force ($\Delta G°$) becomes more negative. The same holds for the monoferrocenyl complexes (last two entries in Table 1). Despite the small sample size, this behavior is not consistent with Marcus inverted region kinetics, leading us to explore other explanations.

The Role of Fc Centered Excited States. To resolve the disagreement between the experimental values for the excited-state lifetimes and the spectroscopic prediction that kinetics for BET should fall into the Marcus inverted region, the role of metal centered Fc states in the excited-state decay kinetics was considered. One possibility is relaxation of the initially formed ^{1}MMCT state by intersystem crossing to a ^{3}Fc (d-d) state. Though this ^{3}Fc state is at a lower energy (9360 cm^{-1})[45] than the ^{1}MMCT states for the Fe^{II}/Ti^{IV} complexes (10900−15900 cm^{-1}, Table S1), the reported lifetime for ^{3}Fc is 90 ns,[46] 3 orders of magnitude longer than the excited-state lifetimes for the complexes herein (18−41 ps). The observed BET lifetimes are much more consistent with those of ^{1}Fc, which we have measured as 7.5 ± 0.6 ps (Figure S19), consistent with reported literature values.[46] The fact that the measured excited-state lifetimes of the Fe^{II}/Ti^{IV} complexes approach that of ^{1}Fc suggests a role for ^{1}Fc in the excited-state decay kinetics. However, the lowest-energy ^{1}Fc (d-d) state (21800 cm^{-1})[47] is at a significantly higher energy than the MMCT transitions for these complexes, such that thermal population of the ^{1}Fc (d-d) state following excitation of the ^{1}MMCT state seems implausible. An alternate explanation is based on our previous TDDFT calculations that suggest the initially formed singlet excited state is not a pure ^{1}MMCT state but rather a state with both ^{1}MMCT and ^{1}Fc character. It is worth noting that the mixing of Fe centered d-d character into CT transitions in complexes with Fc donors and organic acceptors has been previously hypothesized in complexes investigated as NLO chromophores.[7,48,49] Since the lowest-energy ^{1}Fc (d-d) state (21800 cm^{-1})[47] is at higher energy than the MMCT transitions for the Fe^{II}/Ti^{IV} complexes reported herein, increasing the energy of the MMCT state will decrease the energy gap between the two states, thereby increasing the degree of state mixing (Figure 5). Thus, if the pure Fe^{III}/Ti^{III} MMCT state were relatively long-lived, it is conceivable that increased contributions from the short-lived ^{1}Fc state would decrease the observed excited-state lifetime and that this effect might predominate over kinetics associated with the Marcus inverted region. Such a hypothesis predicts that the excited-state lifetime should decrease as the energy of the MMCT state increases, perhaps even approaching that of ^{1}Fc, which is consistent with the data.

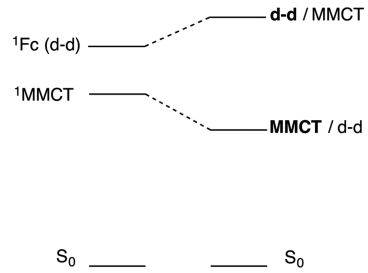

Figure 5. State-mixing diagram showing pure ^{1}MMCT and ^{1}Fc (d-d) states on the left and mixed states on the right. The degree of state mixing is expected to increase as the ^{1}MMCT/^{1}Fc energy gap decreases.

To investigate the hypothesis that the quantity of ^{1}Fc (d-d) state character mixed into the low-energy (LE) excited state increases with the energy of the MMCT transition, DFT and TDDFT[50,51] calculations were carried out using Gaussian 16A.03[52] on the full set of complexes shown in Figure 1. For our previous calculations on a more limited set of complexes, $Cp_2Ti(C_2Fc)_2$ and $Cp^*_2Ti(C_2Fc)_2$,[40] geometry optimization was performed using the ωB97XD/def2-TZV functional[53] and basis,[54] and TDDFT calculations were performed using the B3PW91/6-311+G(d) functional and basis suggested by the Barlow group for D−π−A complexes with a Fc donor and organic acceptors.[49,55−57] Though this model yielded satisfactory results for such a limited set, when tested against the larger set of complexes investigated herein, it failed to predict the observed trends for the energy of the LE band. Using the B3PW91/6-311+G(d) functional and basis for both the geometry optimization and TDDFT resulted in closer agreement between experimental UV−vis spectra and theory (Table 1, Figure 6, Figure S20).

Furthermore, for $Cp_2Ti(C_2Fc)_2CuBr$, a complex which has been structurally characterized,[39] good agreement was obtained between bond distances derived from DFT and those determined from X-ray crystallography (Table S2). We imposed C_2 symmetry on DFT calculations for the $^RCp_2Ti(C_2Fc)_2$ complexes; this constraint improved convergence in the geometry optimization and produced slightly lower energies than were achieved without constraint. The XRD structure for $Cp_2Ti(C_2Fc)_2CuBr$ shows departures from C_2 symmetry; the XRD Cu−C_b distances differ most seriously, both from symmetry equivalence (2.300 and 2.192 Å) and from the computed value (2.355 Å). Several other models were tested, including the functionals ωB97XD[53] and MO6−2X[58] and the basis sets def2-tzvp[59,60] and cc-pVDZ.[61] None of the alternatives were consistently superior to the model suggested by Barlow et al.[49] For all calculations, the medium is represented by a Tomasi polarizable continuum[62] assigned the macroscopic dielectric constant of THF, the solvent in which all UV−vis and TRTAS experiments reported herein were performed.

The LE transition cannot be represented as a single excitation from any particular origin to a destination canonical MO, though the HOMO−LUMO excitation plays a prominent role. Natural transition orbitals (NTOs) (Figures 6 and S21−S25) provide a clearer representation of the transition.[63] The NTOs of the LE transition for all Fe^{II}/Ti^{IV} complexes include a dominant origin/destination pair (identifiable by a substantial occupation number, the largest eigenvalue for the density matrix of corresponding orbitals for ground and excited states).

DOI: 10.1021/acs.inorgchem.9b02316
Inorg. Chem. 2019, 58, 15320−15329

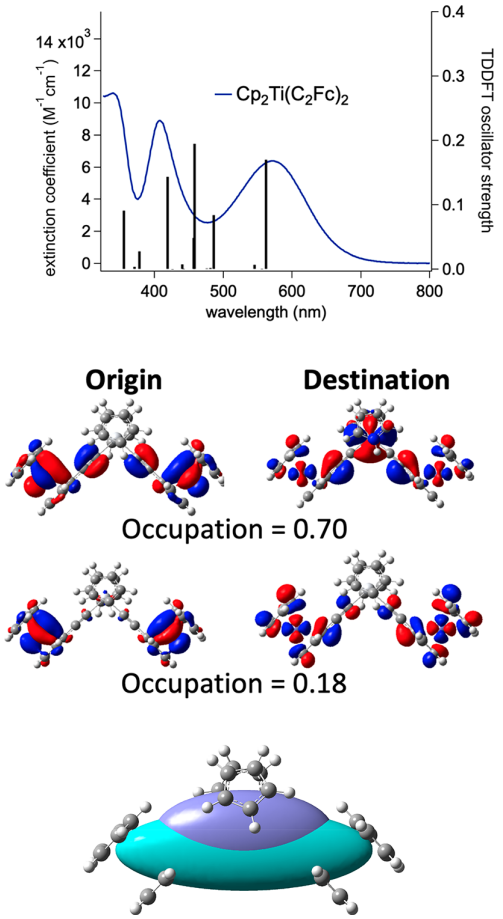

Figure 6. Top: Experimental electronic absorbance spectrum of $Cp_2Ti(C_2Fc)_2$ along with calculated transitions and oscillator strengths (vertical bars). Note: No shift or offset is applied to the calculated transitions. Middle: Diagrams of the origin and destination NTOs with the highest eigenvalues for the lowest-energy transition. Bottom: Diagram depicting the shape of the barycenters for charge accumulation (violet, closest to Ti) and charge depletion (teal, closest to Fe) as calculated by TDDFT for $Cp_2Ti(C_2Fc)_2$. A default isovalue density of 0.0004 is used for all surfaces.

Typically, several smaller eigenvalues are found, suggesting that the excitation includes several components. The NTOs associated with these small eigenvalues we call "minor pairs". Figure 6 shows NTOs for the largest eigenvalue (0.70) and for the second highest eigenvalue (0.18) for $Cp_2Ti(C_2Fc)_2$. For the dominant root, the origin NTO consists predominantly of Fe d-orbitals along with some alkynyl π-orbital character. The destination NTO consists predominantly of Ti d-orbital character; additional amplitude is spread out over the alkyne bridge and the Fe atom. The dominant pair is consistent with the assignment of the LE band as having MMCT character. The minor pair shown is almost entirely localized on the Fc, with significant Fe d-orbital character. Remaining minor pairs are also predominantly Fe d-orbital in character (Figure S21). The NTOs for the remaining complexes reported herein (Figures S22–S25) follow a similar pattern—namely, a dominant NTO pair (MMCT in character) and one or more minor NTO pairs (largely Fe centered). The ratio of the dominant to minor NTO pairs (dom:min, Table 1) demonstrates that for both the diferrocenyl series, and for the monoferrocenyl series, the contribution of the Fe centered minor pairs increases as the energy of the MMCT transition increases. It is worth noting that the presence of the TMS substituents on the Cp rings for the monoferrocenyl complexes, $^{TMS}Cp_2Ti(C_2Fc)(C_2R)$, was necessary for synthetic purposes only[40] and has little effect on the electronic transitions. Chiefly, the TDDFT predicted UV–vis spectra and charge-transfer parameters (*vide infra*) are not significantly impacted by the presence of TMS (Figure S26).

To further quantify the degree of mixing of the ^{1}Fc state with the MMCT state, charge-transfer indices were calculated for the LE excited states using Gaussian[52] and multiwfn.[64] Table 1 gives the values for Q_{CT} (density of charge transferred, a value between 0 and 1 for a one-electron excitation) and D_{CT} (distance between the barycenters of charge-density depletion and accumulation).[65,66] For the series of complexes with two C_2Fc ligands, an increased contribution from the dominant (MMCT) pair of NTOs corresponds with a larger value for Q_{CT}, consistent with a decreased contribution from the localized Fe centered transition. The same trend is observed for the two complexes with only a single C_2Fc ligand. The value of D_{CT} is also noteworthy. The increase in D_{CT} from $Cp^*_2Ti(C_2Fc)_2$ to $Cp_2Ti(C_2Fc)_2$ to $^{MeOOC}Cp_2Ti(C_2Fc)_2$ likely corresponds to greater excited-state charge delocalization onto the $^RCp_2Ti$ fragment as that fragment becomes more electron poor. This is clearly demonstrated by the location of the barycenter for charge accumulation, which progressively shifts closer to the $^RCp_2Ti$ fragment through this series of complexes (Figure S27). The values of D_{CT} for the complexes with only one C_2Fc ligand are significantly longer (3.5–4.2 Å) than the corresponding distances for the complexes with two C_2Fc ligands (1.0–2.1 Å). The shape of the barycenters (Figure 6, bottom) suggests that in these C_2-symmetric systems there are two equivalent sites of charge depletion (each near an Fe atom); thus the resultant charge-transfer vector is the sum of two individual vectors resembling those seen in the one-arm species. Representing the charge transfer as a single vector necessarily averages the positions of charge-depletion, artificially shortening the apparent charge-transfer distance. The positions of the barycenters for charge depletion and accumulation were located on calculated structures of each of the complexes (Figure S27) and indeed show that they lie along the C_2 axis for the symmetric complexes and along the C_2Fc arm for the monoferrocenyl complexes (Figures S27 and S28).

A few additional TRTAS investigations of complexes with Fc donors linked to organic acceptors have revealed similar BET rate constants. For example, for the complex with naphthalenediimide as the acceptor and a 1,4-phenyl spacer, the lifetime for BET was measured as 11 ps.[67] Similarly, with bipyridylboronium acceptors, the observed lifetime is 18 ps, though this can be significantly elongated by rigidifying the system.[68] The aforementioned Fc-ph-DCV BET lifetime was reported as 49 ps.[44] Excited-state mixing with the ^{1}Fc state in these complexes may explain the BET rates, but these investigations report only frontier molecular orbitals at most, precluding such an analysis. A lifetime as short as 0.7 ps has been measured with polychlorotriphenylmethyl radical acceptors and an ethylene spacer, but BET in these systems was shown to occur in the barrierless regime of the Marcus model.[69]

Effect of Copper(I) Coordination. While the original goal of incorporating Cu^I into $^RCp_2Ti(C_2Fc)_2$ complexes was to

DOI: 10.1021/acs.inorgchem.9b02316
Inorg. Chem. 2019, 58, 15320–15329

improve their oxidative stability,[39] the effect of Cu^{I} binding on the photophysics is also worthy of investigation. We have previously reported the electronic absorption spectrum of $Cp_2Ti(C_2Fc)_2$·CuBr (Figure 7) and assigned the LE transition

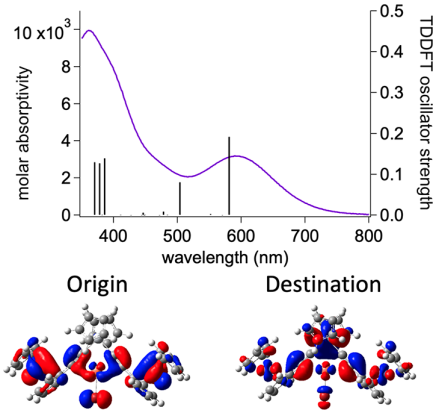

Figure 7. Top: Experimental electronic absorbance spectrum of $Cp_2Ti(C_2Fc)_2CuBr$ along with calculated transitions and oscillator strengths (vertical bars). Note, no shift or offset is applied to the calculated transitions. Bottom: Diagram of the origin and destination NTOs with the highest eigenvalue (0.79) for the lowest-energy transition. For this LE transition, Q_{CT} = 0.67 and D_{CT} = 1.62 Å.

(590 nm) to an $Fe^{II} \rightarrow Ti^{IV}$ MMCT using spectroelectrochemical data.[39] Herein, we report the TDDFT calculated vertical transitions and the dominant NTO pair for the LE transition (Figure 7). The NTOs are consistent with assignment of the LE transition as having significant $Fe^{II} \rightarrow Ti^{IV}$ MMCT character but with a small CuBr orbital contribution to the origin NTO. The TDDFT determined set of three transitions at higher energy than 400 nm has significant Cp → Ti^{IV} LMCT character as demonstrated by the NTOs (Figure S29), consistent with other reported titanocenes.[40,41] However, the NTO for the middle of these three transitions (378 nm) shows significant $Cu^{I} \rightarrow Ti^{IV}$ MMCT character (Figure S29).

The most remarkable impact of Cu^{I} coordination is that, in contrast to the monoexponetial BET of $Cp_2Ti(C_2Fc)_2$, $Cp_2Ti(C_2Fc)_2$·CuBr exhibits three time constants with the longest at 63 ± 1 ns. Shown in Figure 8 are the electronic

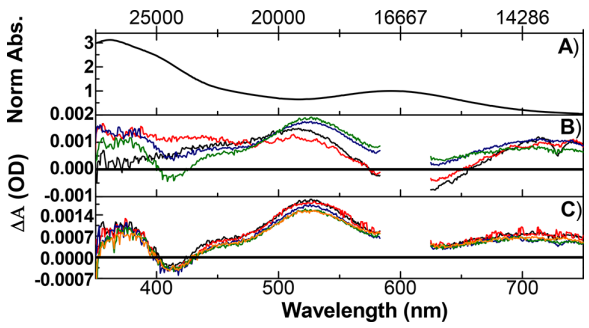

Figure 8. (A) Electronic absorbance spectrum of $Cp_2Ti(C_2Fc)_2$·CuBr. (B) Pump−probe transient spectra collected at 0.4 (black), 1 (red), 10 (blue), and 50 ps (green). (C) Pump−probe transient spectra with 600 nm excitation collected at 50 (black), 500 (red), 1000 (blue), 5000 (green), and 7500 ps (orange).

absorption spectrum for $Cp_2Ti(C_2Fc)_2$·CuBr, early time pump−probe transient absorption spectra (<50 ps), and longer time pump−probe transient absorption spectra persisting until the maximum delay time of the instrument (50−7500 ps). Nanosecond flash-photolysis transient spectra were collected to measure the long decay lifetime (τ_3) past the pump−probe transient absorption maximum delay time (7.5 ns) to show full recovery of the ground state (Figures S15 and S16).

Unlike the parent $Cp_2Ti(C_2Fc)_2$ species, the initial 0.4 and 1 ps transient spectra feature only one ground-state bleach from 558 to 673 nm corresponding to the loss of the $Fe^{II} \rightarrow Ti^{IV}$ MMCT with two induced excited-state absorptions now stretching from 350 to 558 nm and from 673 to 740 nm. Based on our previous measurements of the $^{R}Cp_2Ti(C_2Fc)_2$ complexes, we ascribe the induced excited-state absorption from 450 to 550 nm to the $Ti^{III} \rightarrow$ Cp or $Ti^{III} \rightarrow C_2Cp$ MLCT and the 650 to >750 nm absorption to the $C_2Cp \rightarrow Fe^{III}$ LMCT. Best outlined in the 1 ps transient spectra (Figure 8B, red) is a new induced excited-state absorption from ∼400 to 450 nm, which is not present in the $^{R}Cp_2Ti(C_2Fc)_2$ complexes and eclipses the Cp → Ti^{IV} LMCT bleach that should be present in the same region. We believe that this transition originates from a CuBr → Fe^{III} or CuBr → C_2Cp charge transfer, as there are no other major structural modifications from the $^{R}Cp_2Ti(C_2Fc)_2$ complexes. The transient spectra at delay times longer than 50 ps are clearly different from the 1 ps transient spectrum, and unlike the complexes without CuBr, these new features do not decay within the maximum delay time of the instrument. Chiefly, the spectra feature a new bleach from 397 to 425 nm as well as three induced excited-state absorptions from <350 to 397 nm, 425 to 640 nm, and 640 to >750 nm. The evolution of the excited-state absorption spectra in the first 50 ps is accompanied by isosbestic points at 488 and 688 nm and a slight red-shift of the excited-state absorption maximum at ∼516 to ∼525 nm. Of significant interest is that the spectra at longer delay times do not show a ground-state bleach of the $Fe^{II} \rightarrow Ti^{IV}$ MMCT transition, suggesting that a higher-intensity transition is eclipsing this transition (reverse saturable absorption effect).

Multiexponential decay fitting of the observed pump−probe experiment global kinetic trace produced two time constants of 4.5 (fixed) and 20 ± 10 ps. The third, final time constant (when the ΔA returns to 0) is measured by nanosecond flash-photolysis to be 63 ± 1 ns. The first time constant (τ_1, 4.5 ps) is ascribed to the relaxation of the lowest ^{1}MMCT excited state from the Franck−Condon state with the electronic configuration of $Ti^{III}-Fe^{III}-Cu^{I}$. This assignment is made by again comparing the similarities of the initial $Cp_2Ti(C_2Fc)_2$·CuBr transient spectra (Ti^{III} MLCT and Fe^{III} LMCT) with those of the $^{R}Cp_2Ti(C_2Fc)_2$ complexes. Assignment of the other time constants (τ_2 and τ_3) proves to be more challenging. One clue to the possible assignment of the long-lived (τ_3 = 63 ns) state is that ^{3}Fc is known to be long-lived with strong absorbance at long wavelengths (τ_{T1} of ∼90 ns, ε_{T1} ∼ 5700 M^{-1} cm^{-1} at 700 nm).[46] Such a state could be responsible for both the observed magnitude of τ_3 and the long-wavelength transient absorption (positive ΔA). This suggests a model where τ_2 (20 ps) is assigned to intersystem crossing (ISC) from the initially formed ^{1}MMCT state ($Ti^{III}-Fe^{III}-Cu^{I}$) to a triplet state ($Ti^{IV}-{}^{3}Fe^{II}-Cu^{I}$), and τ_3 (63 ns) is assigned to relaxation from T_1 back to the ground state (Figure 9). The observation of isosbestic points associated with τ_2 is consistent with an ISC

DOI: 10.1021/acs.inorgchem.9b02316
Inorg. Chem. 2019, 58, 15320−15329

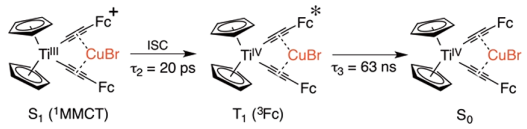

Figure 9. Scheme showing excited-state evolution from the ^{1}MMCT state. ISC is essentially BET that leaves the Fc in a triplet excited-state. That triplet state essentially relaxes with similar excited state dynamics to that of native ^{3}Fc.

event. Furthermore, since ISC is essentially a BET process that leaves the Fe in a triplet state, the similar value of τ_2 to the BET lifetimes of the complexes without coordinated CuBr is not surprising.

Again, to investigate the hypothesis of an iron centered triplet species (Ti^{IV}–$^3Fe^{II}$–Cu^{I}), we performed an unrestricted DFT optimization of the lowest-energy triplet excited state using the same B3PW91/6-311+G(d) functional and basis suggested by Barlow[49] with a symmetry reduction to C_1 as would be anticipated for a localized excited state. Indeed, the uDFT optimization of T_1 (sum of Mulliken spin densities is 2) calculated a structure where one of the iron atoms features a spin density of 2 while all other atoms have a spin density of <0.1. Moreover, uTD-DFT calculation (Figure 10) of the optimized T_1 structures features new transitions at 954, 830, and 595 nm with high oscillator strength (~0.199, ~0.042, ~0.175, respectively). Reasonable agreement between the experimental ΔA and calculated T_1 spectra is observed with the calculation exhibiting an ~2000 cm^{-1} red-shift. NTO

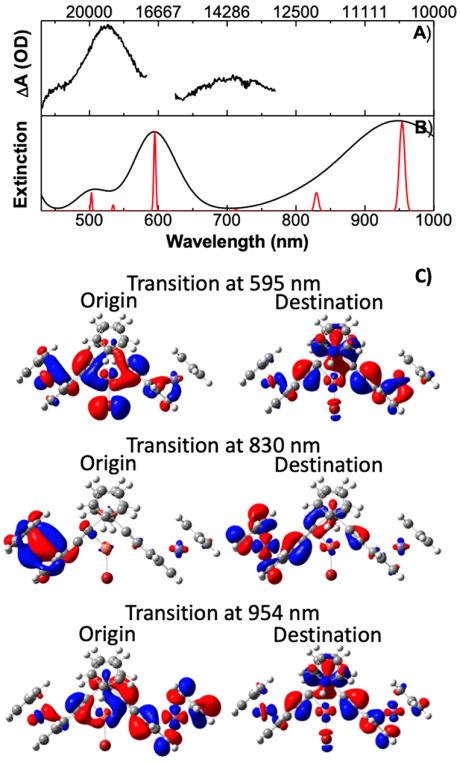

Figure 10. (A) Experimental pump–probe transient absorption spectrum of $Cp_2Ti(C_2Fc)_2CuBr$ at a 50 ps time delay. (B) ^{3}TDDFT calculated spectrum (assuming a fwhm of 2000 cm-1). (C) NTOs for selected triplet transitions.

calculations corresponding to the above transitions (Figure 10) reveal the transition at 954 nm is predominantly a $^3Fe \rightarrow Ti^{IV}$ transition, the transition at 830 nm is predominantly a ^{1}Fe localized d-d transition, and the transition at 595 nm is predominantly a mix of ^{1}Fe (localized on non-^{3}Fe) $\rightarrow Ti^{IV}$ and CuBr $\rightarrow Ti^{IV}$ charge transfer. The confirmation from the uDFT and TDDFT of an iron centered triplet state explains the lack of $Fe^{II} \rightarrow Ti^{IV}$ MMCT bleach in the observed transient spectra. Chiefly, ^{3}Fc species are known to exhibit high extinction ESA from 500 to >800 nm.[46] Also, such a T_1 state returns Ti to a Ti^{IV} state, once again allowing CT to Ti^{IV} transitions. Both of these may contribute to the eclipse of the bleach.

We investigated why ISC to ^{3}Fe is competitive with BET in the CuBr coordination complexes and not the parent species. One hypothesis is that spin–orbit coupling of the Br (spin–orbit coupling constant (ζ) = 3385 cm^{-1} Br (4p),[70] is assisting the ISC to the ^{3}Fc state. To test this hypothesis, the chloride analogue, $Cp_2Ti(C_2Fc)_2$·CuCl (ζ = 882 cm^{-1} Cl (3p))[71] was examined by nanosecond flash-photolysis. The CuCl complex steady-state UV–visible spectra and spectroelectrochemistry have been previously reported and are nearly identical to the CuBr complex.[39] Similarly, the flash-photolysis transient absorption spectra and lifetime are statistically identical to the CuBr complex (Figure S18). Because the transient lifetime data do not show statistical differences, we believe that the halogen is not dominant in facilitating ISC, suggesting a role for Cu^{I}. In support of this suggestion, the coordination of Zn^{II} has recently been proposed to enhance ISC in porphyrin-ferrocene conjugates.[72]

Lastly, we considered a role for a charge-shift process, namely that after $Fe^{II} \rightarrow Ti^{IV}$ CT, a charge-shift from Cu^{I} to Fe^{III} might occur (ground-state oxidation of Cu^{I} complexes by ferricenium is known).[73] However, previous electrochemical investigations in our group have shown that the oxidation of Cu^{I} in a very similar coordination environment, i.e., $Cp_2Ti(C_2Ph)_2CuBr$, was not observed in the window investigated.[39] This suggests that the $Cu^{II/I}$ potential is at least 400 mV anodic of the $Fe^{III/II}$ potential, rendering such a charge-shift unlikely.

CONCLUSION

A series of Fc-alkynyl bridge-Ti^{IV} complexes with high-molar absorptivity $Fe^{II} \rightarrow Ti^{IV}$ MMCT transitions has been investigated using both TRTAS and TDDFT calculations. The excited-state lifetimes range from 18 to 41 ps, and the excited-state absorptions associated with this decay are consistent with the formulation of an Fe^{III}/Ti^{III} excited state. Thus, these lifetimes are ascribed to BET. Spectroscopic evidence suggests that BET should fall into the Marcus inverted region. However, the trend in lifetimes for this series of complexes, where $\Delta G°$ for BET ranges from −1.97 to −1.35 eV, does not follow this behavior. Chiefly, the complexes with the highest-energy MMCT states have the shortest excited-state lifetimes. The similarity of the observed excited-state lifetimes with that of ^{1}Fc suggests its decay may play a significant role in the excited-state kinetics. Herein, a model is suggested whereby the lifetime of the ^{1}MMCT excited state is shortened by increased ^{1}Fc character admixed with the initially formed ^{1}MMCT state. Indeed, TDDFT calculations are consistent with there being greater ^{1}Fc character mixed into the ^{1}MMCT transition for those complexes with the highest energy. Though several authors have hypothesized that CT transitions for complexes with Fc donors are contaminated

DOI: 10.1021/acs.inorgchem.9b02316
Inorg. Chem. 2019, 58, 15320–15329

with ^{1}Fc character,[48,49,74] this investigation suggests that this character can impact the excited-state behavior. Furthermore, whereas most design strategies for extending the lifetimes of CT excited states in metal complexes focus on eliminating lower-lying metal centered excited-states,[14,32,75] this study suggests that higher-lying metal centered excited states might also impact excited state dynamics.

The coordination of CuX between the alkynes led to the remarkable result that the excited-state lifetime increased by 3 orders of magnitude. The spectroscopic and computational data are consistent with this long-lived species being a Fc centered triplet excited state, formed by ISC from the initially formed singlet state. It is not apparent why Cu^I would facilitate ISC. We are presently working on the preparation of complexes with transition metals other than Cu coordinated between the alkynes in order to investigate their excited-state behavior.

■ ASSOCIATED CONTENT

Supporting Information

The Supporting Information is available free of charge on the ACS Publications website at DOI: 10.1021/acs.inorgchem.9b02316.

Materials, description of instrumentation, synthetic details for $^{MeOOC}Cp_2Ti(C_2Fc)_2$, cyclic voltammogram of $^{MeOOC}Cp_2Ti(C_2Fc)_2$, determination of ΔG, table of steady-state spectroscopic parameters, extinction spectra of $^{MeOOC}Cp_2Ti(C_2Fc)_2$ and $Cp_2Ti(C_2Fc)_2CuBr$, pump−probe transient absorption spectra at set time delays for all complexes, pump−probe transient absorption single-wavelength kinetic fitting for all complexes, pump−probe transient absorption global fitting analysis and time correlated spectra for all complexes, nanosecond flash-photolysis transient absorption spectra and single-wavelength kinetics for $Cp_2Ti(C_2Fc)_2CuBr$ and $Cp_2Ti(C_2Fc)_2CuCl$, pump−probe transient absorption of ferrocene, spectra for all complexes with overlaid TD-DFT vertical transitions, comparison of DFT optimized and $Cp_2Ti(C_2Fc)_2CuBr$ structure, NTOs for select transitions for all complexes in Figure 1, and xyz coordinates of all DFT calculated structures (PDF)

Structure of $Cp_2Ti(C_2Fc)_2$ (XYZ)

■ AUTHOR INFORMATION

Corresponding Authors

*E-mail: paul.wagenknecht@furman.edu (P.S.W.).

*E-mail: jrack@unm.edu (J.J.R.).

ORCID

Jeffrey J. Rack: 0000-0001-6121-879X

Notes

The authors declare no competing financial interest.

■ ACKNOWLEDGMENTS

This work was supported by the National Science Foundation under Grants CHE-1362516 (P.S.W.) and CHE-1602240 (J.J.R.) and in part through the EPSCoR Program under NSF Award #OIA-1655740. Any opinions, findings, and conclusions or recommendations expressed in this material are those of the author(s) and do not necessarily reflect those of the National Science Foundation. M.D.T. was supported by the Arnold and Mabel Beckman Foundation Beckman Scholars Award. Z.A. thanks BAPKO, the research support office of Marmara University.

■ REFERENCES

(1) Ashford, D. L.; Gish, M. K.; Vannucci, A. K.; Brennaman, M. K.; Templeton, J. L.; Papanikolas, J. M.; Meyer, T. J. Molecular Chromophore-Catalyst Assemblies for Solar Fuel Applications. *Chem. Rev.* **2015**, *115* (23), 13006−13049.

(2) Morseth, Z. A.; Wang, L.; Puodziukynaite, E.; Leem, G.; Gilligan, A. T.; Meyer, T. J.; Schanze, K. S.; Reynolds, J. R.; Papanikolas, J. M. Ultrafast Dynamics in Multifunctional Ru(II)-Loaded Polymers for Solar Energy Conversion. *Acc. Chem. Res.* **2015**, *48* (3), 818−827.

(3) Ji, J.-M.; Zhou, H.; Kim, H. K. Rational design criteria for D-π-A structured organic and porphyrin sensitizers for highly efficient dye-sensitized solar cells. *J. Mater. Chem. A* **2018**, *6* (30), 14518−14545.

(4) Twilton, J.; Le, C.; Zhang, P.; Shaw, M. H.; Evans, R. W.; MacMillan, D. W. C. The merger of transition metal and photocatalysis. *Nature Reviews Chemistry* **2017**, *1*, 0052.

(5) Prier, C. K.; Rankic, D. A.; MacMillan, D. W. C. Visible Light Photoredox Catalysis with Transition Metal Complexes: Applications in Organic Synthesis. *Chem. Rev.* **2013**, *113* (7), 5322−5363.

(6) Nelson, J. N.; Zhang, J.; Zhou, J.; Rugg, B. K.; Krzyaniak, M. D.; Wasielewski, M. R. Effect of Electron-Nuclear Hyperfine Interactions on Multiple-Quantum Coherences in Photogenerated Covalent Radical (Qubit) Pairs. *J. Phys. Chem. A* **2018**, *122* (49), 9392−9402.

(7) Kaur, S.; Kaur, M.; Kaur, P.; Clays, K.; Singh, K. Ferrocene chromophores continue to inspire. Fine-tuning and switching of the second-order nonlinear optical response. *Coord. Chem. Rev.* **2017**, *343*, 185−219.

(8) Morseth, Z. A.; Pho, T. V.; Gilligan, A. T.; Dillon, R. J.; Schanze, K. S.; Reynolds, J. R.; Papanikolas, J. M. Role of Macromolecular Structure in the Ultrafast Energy and Electron Transfer Dynamics of a Light-Harvesting Polymer. *J. Phys. Chem. B* **2016**, *120* (32), 7937−7948.

(9) Castellano, F. N. Altering Molecular Photophysics by Merging Organic and Inorganic Chromophores. *Acc. Chem. Res.* **2015**, *48* (3), 828−839.

(10) Ko, C.-C.; Yam, V. W.-W. Coordination Compounds with Photochromic Ligands: Ready Tunability and Visible Light-Sensitized Photochromism. *Acc. Chem. Res.* **2018**, *51* (1), 149−159.

(11) Lo, K. K.-W. Luminescent Rhenium(I) and Iridium(III) Polypyridine Complexes as Biological Probes, Imaging Reagents, and Photocytotoxic Agents. *Acc. Chem. Res.* **2015**, *48* (12), 2985−2995.

(12) Whittemore, T. J.; Millet, A.; Sayre, H. J.; Xue, C.; Dolinar, B. S.; White, E. G.; Dunbar, K. R.; Turro, C. Tunable Rh2(II,II) Light Absorbers as Excited-State Electron Donors and Acceptors Accessible with Red/Near-Infrared Irradiation. *J. Am. Chem. Soc.* **2018**, *140* (15), 5161−5170.

(13) Wu, S.-H.; Ling, J.-W.; Lai, S.-H.; Huang, M.-J.; Cheng, C. H.; Chen, I. C. Dynamics of the Excited States of [Ir(ppy)2bpy]+ with Triple Phosphorescence. *J. Phys. Chem. A* **2010**, *114* (38), 10339−10344.

(14) Wagenknecht, P. S.; Ford, P. C. Metal Centered Ligand Field Excited States: Their Roles in the Design and Performance of Transition Metal Based Photochemical Molecular Devices. *Coord. Chem. Rev.* **2011**, *255* (5), 591−616.

(15) McCusker, J. K. Electronic structure in the transition metal block and its implications for light harvesting. *Science* **2019**, *363* (6426), 484.

(16) Ashley, D. C.; Jakubikova, E. Tuning the Redox Potentials and Ligand Field Strength of Fe(II) Polypyridines: The Dual π-Donor and π-Acceptor Character of Bipyridine. *Inorg. Chem.* **2018**, *57* (16), 9907−9917.

(17) Chergui, M. On the interplay between charge, spin and structural dynamics in transition metal complexes. *Dalton Transactions* **2012**, *41* (42), 13022−13029.

(18) Yaghoobi Nia, N.; Farahani, P.; Sabzyan, H.; Zendehdel, M.; Oftadeh, M. A Combined Computational and Experimental Study of the [Co(bpy)3]2+/3+ Complexes as One-Electron Outer-Sphere

DOI: 10.1021/acs.inorgchem.9b02316
Inorg. Chem. 2019, 58, 15320−15329

Redox Couples in Dye-Sensitized Solar Cell Electrolyte Media. *Phys. Chem. Chem. Phys.* **2014**, *16* (23), 11481−11491.
(19) Ravetz, B. D.; Wang, J. Y.; Ruhl, K. E.; Rovis, T. Photoinduced Ligand-to-Metal Charge Transfer Enables Photocatalyst-Independent Light-Gated Activation of Co(II). *ACS Catal.* **2019**, *9* (1), 200−204.
(20) Brauchli, S. Y.; Malzner, F. J.; Constable, E. C.; Housecroft, C. E. Copper(i)-based dye-sensitized solar cells with sterically demanding anchoring ligands: bigger is not always better. *RSC Adv.* **2015**, *5* (60), 48516−48525.
(21) Ilmi, R.; Juma Al-Busaidi, I.; Haque, A.; Khan, M. S. Recent progress in coordination chemistry, photo-physical properties, and applications of pyridine-based Cu(I) complexes. *J. Coord. Chem.* **2018**, *71* (19), 3045−3076.
(22) Katsoukis, G.; Frei, H. Heterobinuclear Light Absorber Coupled to Molecular Wire for Charge Transport across Ultrathin Silica Membrane for Artificial Photosynthesis. *ACS Appl. Mater. Interfaces* **2018**, *10* (37), 31422−31432.
(23) Han, H.; Frei, H. In Situ Spectroscopy of Water Oxidation at Ir Oxide Nanocluster Driven by Visible TiOCr Charge-transfer Chromophore in Mesoporous Silica. *J. Phys. Chem. C* **2008**, *112* (41), 16156−16159.
(24) Auböck, G.; Chergui, M. Sub-50-fs Photoinduced Spin Crossover in [Fe(bpy)3]2+. *Nat. Chem.* **2015**, *7* (8), 629−633.
(25) Du, L.; Lan, Z. Ultrafast Structural Flattening Motion in Photoinduced Excited State Dynamics of a Bis(diimine) Copper(I) Complex. *Phys. Chem. Chem. Phys.* **2016**, *18* (11), 7641−7650.
(26) Iwamura, M.; Takeuchi, S.; Tahara, T. Ultrafast Excited-State Dynamics of Copper(I) Complexes. *Acc. Chem. Res.* **2015**, *48* (3), 782−791.
(27) McClure, B. A.; Frei, H. Excited State Electron Transfer of All-Inorganic Heterobinuclear TiOMn2+ Chromophore Anchored on Silica Nanoparticle Surface. *J. Phys. Chem. C* **2014**, *118* (22), 11601−11611.
(28) McCusker, C. E.; Castellano, F. N. Design of a Long-Lifetime, Earth-Abundant, Aqueous Compatible Cu(I) Photosensitizer Using Cooperative Steric Effects. *Inorg. Chem.* **2013**, *52* (14), 8114−8120.
(29) Higgins, R. F.; Fatur, S. M.; Damrauer, N. H.; Ferreira, E. M.; Rappé, A. K.; Shores, M. P. Detection of an Energy-Transfer Pathway in Cr-Photoredox Catalysis. *ACS Catal.* **2018**, *8* (10), 9216−9225.
(30) Büldt, L. A.; Wenger, O. S. Chromium complexes for luminescence, solar cells, photoredox catalysis, upconversion, and phototriggered NO release. *Chemical Science* **2017**, *8* (11), 7359−7367.
(31) Otto, S.; Dorn, M.; Förster, C.; Bauer, M.; Seitz, M.; Heinze, K. Understanding and exploiting long-lived near-infrared emission of a molecular ruby. *Coord. Chem. Rev.* **2018**, *359*, 102−111.
(32) Chábera, P.; Liu, Y.; Prakash, O.; Thyrhaug, E.; Nahhas, A. E.; Honarfar, A.; Essén, S.; Fredin, L. A.; Harlang, T. C. B.; Kjær, K. S.; Handrup, K.; Ericson, F.; Tatsuno, H.; Morgan, K.; Schnadt, J.; Häggström, L.; Ericsson, T.; Sobkowiak, A.; Lidin, S.; Huang, P.; Styring, S.; Uhlig, J.; Bendix, J.; Lomoth, R.; Sundström, V.; Persson, P.; Wärnmark, K. A low-spin Fe(iii) complex with 100-ps ligand-to-metal charge transfer photoluminescence. *Nature* **2017**, *543*, 695.
(33) Shields, B. J.; Kudisch, B.; Scholes, G. D.; Doyle, A. G. Long-Lived Charge-Transfer States of Nickel(II) Aryl Halide Complexes Facilitate Bimolecular Photoinduced Electron Transfer. *J. Am. Chem. Soc.* **2018**, *140* (8), 3035−3039.
(34) Lim, C.-H.; Kudisch, M.; Liu, B.; Miyake, G. M. C-N Cross-Coupling via Photoexcitation of Nickel-Amine Complexes. *J. Am. Chem. Soc.* **2018**, *140* (24), 7667−7673.
(35) Hernandez-Perez, A. C.; Collins, S. K. Heteroleptic Cu-Based Sensitizers in Photoredox Catalysis. *Acc. Chem. Res.* **2016**, *49* (8), 1557−1565.
(36) Pirtsch, M.; Paria, S.; Matsuno, T.; Isobe, H.; Reiser, O. [Cu(dap)2Cl] As an Efficient Visible-Light-Driven Photoredox Catalyst in Carbon-Carbon Bond-Forming Reactions. *Chem. - Eur. J.* **2012**, *18* (24), 7336−7340.
(37) Liu, Y.; Yiu, S.-C.; Ho, C.-L.; Wong, W.-Y. Recent advances in copper complexes for electrical/light energy conversion. *Coord. Chem. Rev.* **2018**, *375*, 514−557.
(38) Garakyaraghi, S.; McCusker, C. E.; Khan, S.; Koutnik, P.; Bui, A. T.; Castellano, F. N. Enhancing the Visible-Light Absorption and Excited-State Properties of Cu(I) MLCT Excited States. *Inorg. Chem.* **2018**, *57* (4), 2296−2307.
(39) Pienkos, J. A.; Webster, A. B.; Piechota, E. J.; Agakidou, A. D.; McMillen, C. D.; Pritchett, D. Y.; Meyer, G. J.; Wagenknecht, P. S. Oxidatively stable ferrocenyl-π-bridge-titanocene D-π-A complexes: an electrochemical and spectroscopic investigation of the mixed-valent states. *Dalton Transactions* **2018**, *47*, 10953−10964.
(40) Turlington, M. D.; Pienkos, J. A.; Carlton, E. S.; Wroblewski, K. N.; Myers, A. R.; Trindle, C. O.; Altun, Z.; Rack, J. J.; Wagenknecht, P. S. Complexes with Tunable Intramolecular Ferrocene to TiIV Electronic Transitions: Models for Solid State FeII to TiIV Charge Transfer. *Inorg. Chem.* **2016**, *55* (5), 2200−2211.
(41) Harrigan, R. W.; Hammond, G. S.; Gray, H. B. Photochemistry of titanocene(IV) derivatives. *J. Organomet. Chem.* **1974**, *81* (1), 79−85.
(42) Coutts, R. S. P.; Wailes, P. C.; Martin, R. L. Dimeric dicyclopentadienyltitanium(III) halides. *J. Organomet. Chem.* **1973**, *47* (2), 375−382.
(43) Cuffe, L.; Hudson, R. D. A.; Gallagher, J. F.; Jennings, S.; McAdam, C. J.; Connelly, R. B. T.; Manning, A. R.; Robinson, B. H.; Simpson, J. Synthesis, Structure, and Redox Chemistry of Ethenyl and Ethynyl Ferrocene Polyaromatic Dyads. *Organometallics* **2005**, *24* (9), 2051−2060.
(44) Mohammed, O. F.; Sarhan, A. A. O. Ultrafast excited-state dynamics of ferrocene-bridge-acceptor system. *Chem. Phys.* **2010**, *372* (1), 17−21.
(45) Araki, Y.; Yasumura, Y.; Ito, O. Photoinduced Electron Transfer Competitive with Energy Transfer of the Excited Triplet State of [60]Fullerene to Ferrocene Derivatives Revealed by Combination of Transient Absorption and Thermal Lens Measurements. *J. Phys. Chem. B* **2005**, *109*, 9843−9848.
(46) Scuppa, S.; Orian, L.; Dini, D.; Santi, S.; Meneghetti, M. Nonlinear Absorption Properties and Excited State Dynamics of Ferrocene. *J. Phys. Chem. A* **2009**, *113* (33), 9286−9294.
(47) Fery-Forgues, S.; Delavaux-Nicot, B. Ferrocene and ferrocenyl derivatives in luminescent systems. *J. Photochem. Photobiol., A* **2000**, *132* (3), 137−159.
(48) Kanis, D. R.; Ratner, M. A.; Marks, T. J. Calculation and electronic description of quadratic hyperpolarizabilities. Toward a molecular understanding of NLO responses in organotransition metal chromophores. *J. Am. Chem. Soc.* **1992**, *114* (26), 10338−10357.
(49) Salman, S.; Brédas, J.-L.; Marder, S. R.; Coropceanu, V.; Barlow, S. Dipolar Ferrocene and Ruthenocene Second-Order Nonlinear Optical Chromophores: A Time-Dependent Density Functional Theory Investigation of Their Absorption Spectra. *Organometallics* **2013**, *32* (20), 6061−6068.
(50) Casida, M. E.; Jamorski, C.; Casida, K. C.; Salahub, D. R. Molecular excitation energies to high-lying bound states from time-dependent density-functional response theory: Characterization and correction of the time-dependent local density approximation ionization threshold. *J. Chem. Phys.* **1998**, *108* (11), 4439−4449.
(51) Bauernschmitt, R.; Ahlrichs, R. Treatment of electronic excitations within the adiabatic approximation of time dependent density functional theory. *Chem. Phys. Lett.* **1996**, *256* (4), 454−464.
(52) Frisch, M. J.; Trucks, G. W.; Schlegel, H. B.; Scuseria, G. E.; Robb, M. A.; Cheeseman, J. R.; Scalmani, G.; Barone, V.; Petersson, G. A.; Nakatsuji, H.; Li, X.; Caricato, M.; Marenich, A. V.; Bloino, J.; Janesko, B. G.; Gomperts, R.; Mennucci, B.; Hratchian, H. P.; Ortiz, J. V.; Izmaylov, A. F.; Sonnenberg, J. L.; Williams; Ding, F.; Lipparini, F.; Egidi, F.; Goings, J.; Peng, B.; Petrone, A.; Henderson, T.; Ranasinghe, D.; Zakrzewski, V. G.; Gao, J.; Rega, N.; Zheng, G.; Liang, W.; Hada, M.; Ehara, M.; Toyota, K.; Fukuda, R.; Hasegawa, J.; Ishida, M.; Nakajima, T.; Honda, Y.; Kitao, O.; Nakai, H.; Vreven, T.; Throssell, K.; Montgomery, J. A., Jr.; Peralta, J. E.; Ogliaro, F.;

DOI: 10.1021/acs.inorgchem.9b02316
Inorg. Chem. 2019, 58, 15320−15329

Bearpark, M. J.; Heyd, J. J.; Brothers, E. N.; Kudin, K. N.; Staroverov, V. N.; Keith, T. A.; Kobayashi, R.; Normand, J.; Raghavachari, K.; Rendell, A. P.; Burant, J. C.; Iyengar, S. S.; Tomasi, J.; Cossi, M.; Millam, J. M.; Klene, M.; Adamo, C.; Cammi, R.; Ochterski, J. W.; Martin, R. L.; Morokuma, K.; Farkas, O.; Foresman, J. B.; Fox, D. J.; *Gaussian, Inc.*: revision A.03, Wallingford, CT, 2016.

(53) Chai, J.-D.; Head-Gordon, M. Long-range corrected hybrid density functionals with damped atom-atom dispersion corrections. *Phys. Chem. Chem. Phys.* **2008**, *10* (44), 6615−6620.

(54) Weigend, F.; Ahlrichs, R. Balanced basis sets of split valence, triple zeta valence and quadruple zeta valence quality for H to Rn: Design and assessment of accuracy. *Phys. Chem. Chem. Phys.* **2005**, *7* (18), 3297−3305.

(55) Perdew, J. P.; Chevary, J. A.; Vosko, S. H.; Jackson, K. A.; Pederson, M. R.; Singh, D. J.; Fiolhais, C. Atoms, molecules, solids, and surfaces: Applications of the generalized gradient approximation for exchange and correlation. *Phys. Rev. B: Condens. Matter Mater. Phys.* **1992**, *46* (11), 6671−6687.

(56) Becke, A. D. Density functional thermochemistry. III. The role of exact exchange. *J. Chem. Phys.* **1993**, *98* (7), 5648−5652.

(57) Perdew, J. P.; Burke, K.; Wang, Y. Generalized gradient approximation for the exchange-correlation hole of a many-electron system. *Phys. Rev. B: Condens. Matter Mater. Phys.* **1996**, *54* (23), 16533−16539.

(58) Zhao, Y.; Truhlar, D. G. The M06 suite of density functionals for main group thermochemistry, thermochemical kinetics, noncovalent interactions, excited states, and transition elements: two new functionals and systematic testing of four M06-class functionals and 12 other functionals. *Theor. Chem. Acc.* **2008**, *120* (1), 215−241.

(59) Woon, D.; Dunning, T. Gaussian Basis Sets for Use in Correlated Molecular Calculations. III. The Atoms Aluminum through Argon. *J. Chem. Phys.* **1993**, *98*, 1358−1371.

(60) Dunning, T. H. Gaussian basis sets for use in correlated molecular calculations. I. The atoms boron through neon and hydrogen. *J. Chem. Phys.* **1989**, *90* (2), 1007−1023.

(61) Balabanov, N. B.; Peterson, K. A. Systematically convergent basis sets for transition metals. I. All-electron correlation consistent basis sets for the 3d elements Sc-Zn. *J. Chem. Phys.* **2005**, *123* (6), 064107.

(62) Tomasi, J.; Mennucci, B.; Cammi, R. Quantum Mechanical Continuum Solvation Models. *Chem. Rev.* **2005**, *105* (8), 2999−3094.

(63) Martin, R. L. Natural transition orbitals. *J. Chem. Phys.* **2003**, *118* (11), 4775−4777.

(64) Lu, T.; Chen, F. Multiwfn: A multifunctional wavefunction analyzer. *J. Comput. Chem.* **2012**, *33* (5), 580−592.

(65) Le Bahers, T.; Adamo, C.; Ciofini, I. A Qualitative Index of Spatial Extent in Charge-Transfer Excitations. *J. Chem. Theory Comput.* **2011**, *7* (8), 2498−2506.

(66) Savarese, M.; Guido, C. A.; Brémond, E.; Ciofini, I.; Adamo, C. Metrics for Molecular Electronic Excitations: A Comparison between Orbital- and Density-Based Descriptors. *J. Phys. Chem. A* **2017**, *121* (40), 7543−7549.

(67) Supur, M.; El-Khouly, M. E.; Seok, J. H.; Kay, K.-Y.; Fukuzumi, S. Elongation of Lifetime of the Charge-Separated State of Ferrocene-Naphthalenediimide-[60]Fullerene Triad via Stepwise Electron Transfer. *J. Phys. Chem. A* **2011**, *115*, 14430.

(68) Thomson, M. D.; Novosel, M.; Roskos, H. G.; Müller, T.; Scheibitz, M.; Wagner, M.; Fabrizi de Biani, F.; Zanello, P. Electronic Structure, Photophysics, and Relaxation Dynamics of a Charge Transfer Excited States in Boron-Nitrogen-Bridged Ferrocene-Donor Organic-Acceptor Compounds. *J. Phys. Chem. A* **2004**, *108*, 3281−3291.

(69) Ratera, I.; Sporer, C.; Ruiz-Molina, D.; Ventosa, N.; Baggerman, J.; Brouwer, A. M.; Rovira, C.; Veciana, J. Solvent Tuning from Normal to Inverted Marcus Region of Intramolecular Electron Transfer in Ferrocent-Based Organic Radicals. *J. Am. Chem. Soc.* **2007**, *129*, 6117−6129.

(70) Orr-Ewing, A. J. Perspective: How can ultrafast laser spectroscopy inform the design of new organic photoredox catalysts for chemical and materials synthesis? *Struct. Dyn.* **2019**, *6* (1), 010901.

(71) Abrahamsson, E.; Groenenboom, G. C.; Krems, R. V. Spin-orbit relaxation of Cl(P1/22) and F(P1/22) in a gas of H2. *J. Chem. Phys.* **2007**, *126* (18), 184303.

(72) Melomedov, J.; Ochsmann, J. R.; Meister, M.; Laquai, F.; Heinze, K. Aminoferrocene and Ferrocene Amino Acid As Electron Donors in Modular Porphyrin-Ferrocene and porphyrin-Ferrocene-Porphyrin Conjugates. *Eur. J. Inorg. Chem.* **2014**, *2014*, 2902−2915.

(73) Back, O.; Leppin, J.; Förster, C.; Heinze, K. Photochemistry and Redox Chemistry of an Unsymmetrical Bimetallic Copper(I) Complex. *Inorg. Chem.* **2016**, *55*, 9653−9662.

(74) Barlow, S.; Bunting, H. E.; Ringham, C.; Green, J. C.; Bublitz, G. U.; Boxer, S. G.; Perry, J. W.; Marder, S. R. Studies of the Electronic Structure of Metallocene-Based Second-Order Nonlinear Optical Dyes. *J. Am. Chem. Soc.* **1999**, *121* (15), 3715−3723.

(75) Cho, H.; Strader, M. L.; Hong, K.; Jamula, L.; Gullikson, E. M.; Kim, T. K.; de Groot, F. M. F.; McCusker, J. K.; Schoenlein, R. W.; Huse, N. Ligand-field symmetry effects in Fe(ii) polypyridyl compounds probed by transient X-ray absorption spectroscopy. *Faraday Discuss.* **2012**, *157* (0), 463−474.

DOI: 10.1021/acs.inorgchem.9b02316
Inorg. Chem. 2019, 58, 15320−15329